

Role of gel aging in template-free synthesis of micro and nano-crystalline sodalites

S. M. Pourali¹, A. Samadi-Maybodi^{2*}

¹*Ph.D Student, Analytical Division, Faculty of Chemistry, University of Mazandaran, Babolsar, Iran*

²*Professor, Analytical Division, Faculty of Chemistry, University of Mazandaran, Babolsar, Iran*

* *Corresponding author's Email: samadi@umz.ac.ir*

Article history:

(Received: 17 Aug 2014, Revised: 16 Sep 2014, Accepted: 12 Oct 2014)

ABSTRACT

A facile effective stirring aging at room temperature prior to conventional hydrothermal treatment was employed in the template-free synthesis of micro- and nano-crystalline sodalites with two different initial gel compositions. The effect of initial Si/Al molar ratio, NaOH concentration and stirring aging time were investigated on the morphology and particle size of the synthesised sodalites. The results revealed that applying various stirring aging time can change the proportion of the contaminant phase associated with sodalite and alter the morphology of the sodalite crystals from wool ball-like consisting of nano-threads to cabbage-like with nano-leaves, as well as size distribution of nanocrystalline sodalite. The size of the nanocrystals was in the range of 50-80 nm as observed by FE-SEM and the yield was as high as about 15%.

Keywords: Nanocrystalline Sodalite, Wool ball-like, Cabbage-like, Morphology, Argon isotherm.

1. INTRODUCTION

Sodalites, a class of microporous aluminosilicates with general formula of $M_8[ABO_4]_6X_2$, are built of a six-membered ring (6R) with a pore size of 0.28 nm, and the maximum diameter of the void included in the framework of 0.63 nm [1]. So far, sodalite crystals attracted considerable attention due to their widespread application in hydrogen storage [2-4], semiconductors [5, 6] and pigment occlusion [7]. Nano-sized and micro-sized sodalite crystals could be easily synthesised in presence of organic templates [8-12] or

structure-directing agents (SDAs) [13] through hydrothermal treatment. Nano-sized sodalites have been obtained using SDAs by solid-solid transformation of Al_2O_3 pillared clay in the alkaline solution [14, 15], direct solid transformation of preformed silicate nanocrystals [16], and washing sodium aluminosilicate solution by NaOH solution to remove the amorphous phase [17]. However, removal of SDAs often leads to irreversible aggregation of the nanocrystals and decrease in crystallinity. The yield of zeolite nanocrystals by this approach is

normally lower than ~ 10%, calculated based on silicon source used [18]. Furthermore, SDAs tend to alter Si/Al molar ratio of the final products, thus remarkably affect their application [19]. The organic additives are non-recyclable and their application is costly and requires calcination which results in the production of CO₂ and NO_x pollution problems [20]. Okubo T. et al. reported the hydrothermal synthesis of sodalite nanocrystals without using any organic additives at low temperature [17]. Undoubtedly, the morphology of zeolites is originally related to the framework type and also closely related to the micropore size, crystal size and shape, and directly affects the physicochemical properties of zeolites. Morphological properties of zeolites are particularly important in catalytic applications where the particle shape can have a dramatic effect on the product distribution due to the differences in rates of transport/diffusion and reaction. Recently, great efforts have been directed toward designing zeolites with desired functions by applying nanotechnology. Thus, there has been a great interest in developing synthetic approaches to control crystal size and morphology of zeolites [21-23].

2. EXPERIMENTAL

2.1 Reagents and Materials

Sodium aluminate, sodium metasilicate (H₂O 43%, Na₂O 29%, SiO₂ 28%) and sodium hydroxide were purchased from

Merck (AR grade) and used without further purification. Double distilled water was used throughout the experiments.

2.2 Synthesis

In a typical procedure, sodium aluminate, sodium hydroxide and water were placed in a plastic beaker and heated to 70 °C while stirred to ensure achievement of a homogeneous mixture, and then cooled to room temperature. Sodium metasilicate was dissolved in water, heated to 70 °C and stirred to obtain a homogeneous mixture, then cooled to room temperature. Afterwards, silicate solution was added slowly to the aluminate solution under vigorous stirring. Subsequently, the gel was aged at room temperature for certain time, according to Table 1, with vigorous stirring prior to conventional hydrothermal treatment to get a homogenous gel-mix. Finally, the gel was transferred into a Teflon-lined stainless-steel autoclave, placed in an air-oven maintained at the required temperature. At the end, the precipitates were recovered by centrifugation, washed with double distilled water and dried in air. The gel composition (molar ratio of the used chemicals), synthesis conditions, and resulting solid phases are presented in Table 1. For FE-SEM and argon adsorption-desorption isotherm studies on the samples, the synthesized products were calcined at 600 °C for 2h.

Table 1. Synthesis conditions of the samples

Gel Composition	Al ₂ O ₃	SiO ₂	Na ₂ O	H ₂ O	Stirring aging (samples labeled as)	Temperature	Duration
a	1	10	6	267	0, 20 min, 72 h (S1, S2, S3)	100 °C	48 h
b	1	3.8	2.1	50	0, 1 h, 2.5 h (S4, S5, S6)	100 °C	48 h

2.3 Characterization

Powder X-ray diffraction (XRD) patterns of the as-synthesized samples were recorded on a GBC MMA X-ray diffractometer using Cu K α radiation of wavelength 0.154178 nm at 35.4 KV and 28 mA. Diffraction data were recorded between 5 and 50°2 θ with a scanning speed of 5°/min. The FT-IR spectrum was recorded on a Bruker Tensor 27 Spectrometer.

Field-emission scanning electron microscopy (FE-SEM) images were provided using a HITACHI, S-4160 field-emission electron microscope operating at 15 kV for indicating the morphology of the samples.

The specific surface area was evaluated using the Brunauer–Emmett–Teller (BET) method, and the pore size distribution was calculated from

desorption branches of argon isotherms applying the Barrett–Joyner–Halenda (BJH) method (Quantachrom Nova 2000e, USA).

3. RESULTS AND DISCUSSION

Figure 1 shows the XRD patterns of the zeolites S1 and S4 prepared by two different starting gel compositions (**a** and **b**, Table 1) under same synthetic condition. As it can be seen, Figure 1**a** and 1**b** shows mixed phases of analcime and NaP-1 zeolites prepared under no stirring aging. With gel composition **a**, having higher Si/Al molar ratio (5), zeolite NaP-1 was the dominant phase while for gel composition **b**, having lower Si/Al molar ratio (1.9), both phases showed high degree of crystallinity.

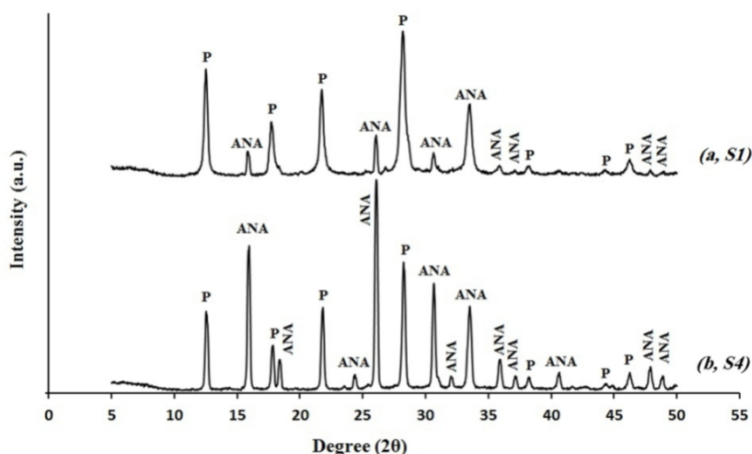


Fig. 1. The XRD patterns of samples S1 and S4 prepared with gel compositions **a** and **b** under no stirring aging.

To further investigate the phase transformation and morphology changes of both gel compositions,

different stirring aging times were employed prior to conventional hydrothermal reaction and the results were followed by XRD and FE-SEM.

First, evolution of gel composition **a** was studied under two different stirring aging time of 20 min and 72 h (S2 and S3, respectively). Fig. 2 illustrates the XRD patterns of the samples S2 and S3 with S2 indicating the formation of a

new phase of sodalite octahydrate zeolite. It also showed a significant decrease in analcime phase comparing to S1 with no stirring aging and a moderate decrease in NaP-1 phase.

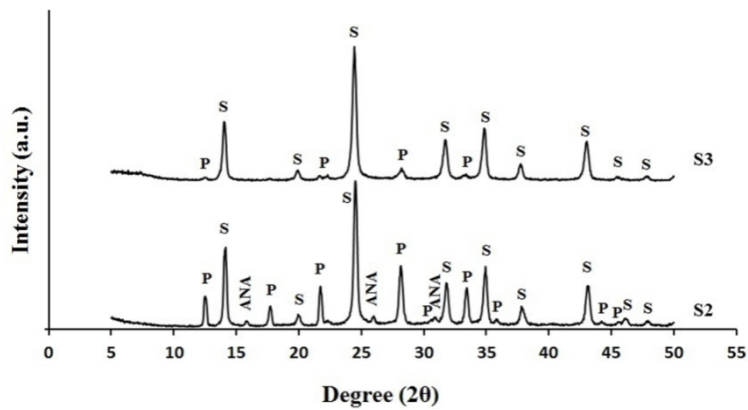


Fig. 2. The XRD patterns of the samples S2 and S3 prepared under 20 min and 72 h stirring aging, from gel composition **a**.

On the other hand, under prolonged stirring aging time of 72 h, the XRD pattern of S3 (Figure 2) showed a dramatic change in phase dominancy with sodalite octahydrate being the dominant phase and NaP-1 zeolite as a remaining impurity phase and no analcime peak was observed. This decrease in NaP-1 and analcime phases

after adding to aging step is the result of their consumption toward the formation of a more pure and stable phase of sodalite octahydrate. After confirming the phase formation by XRD analysis, the morphology and particle size distribution were observed by FE-SEM (Figure 3).

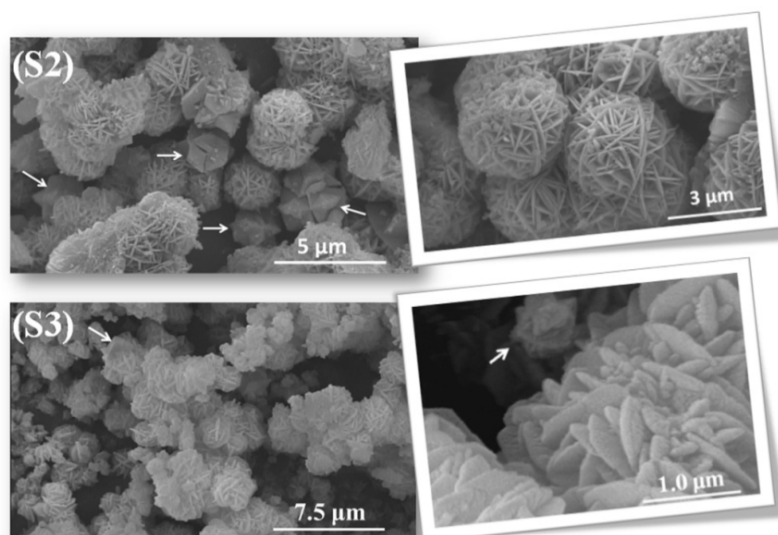


Fig. 3. FE-SEM images of the samples S2 and S3 prepared under 20 min and 72 h stirring aging, using gel composition **a**.

As it can be seen in Figure 3, sample S2 has a wool ball-like morphology and spheres of sodalite aggregate together. The average size of each wool ball is $\sim 3 \mu\text{m}$ with threads having the width range of 80-120 nm. Also, the presence of diamond-like NaP-1 crystals is observable which is in agreement with its XRD pattern (Figure 2, S2). The size of each diamond is about $2 \mu\text{m}$, which are marked with arrows. However, under prolonged aging of 72 h (S3), the morphology of the wool ball-like sodalite changed to well-shaped cabbage-like structures

with an average size of $3 \mu\text{m}$ and leaves in the range of 50-80 nm. Figure 4 illustrates another schematic image of cabbage-like (S3) crystals at higher magnifications showing mainly nano-leaves which are the nano-features of the microcrystals of sodalites. Furthermore, it illustrates that the nano-leaves are connected to each other through an axis, which results in the hierarchical cabbage-like morphology.

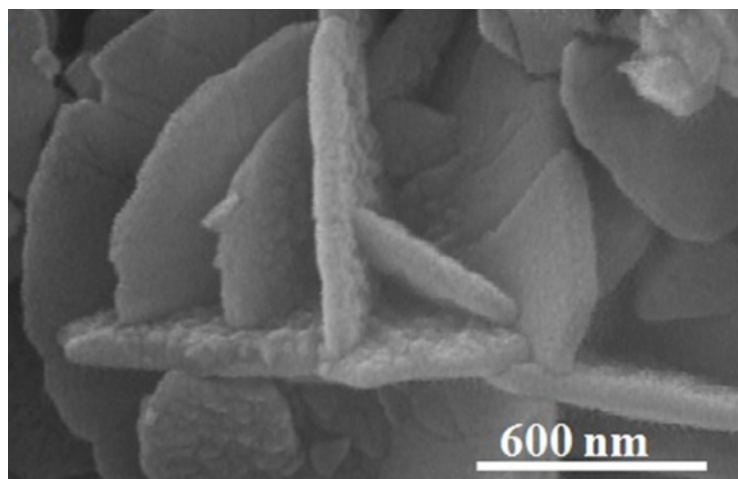


Fig. 4. Nano-leaves of cabbage-like microcrystalline sodalites at 1000X magnification.

Secondly, evolution of gel composition **b** was studied under two different stirring aging of 1 h and 2.5 h (labeled as S5 and S6, respectively). Figure 5 shows the XRD patterns of mentioned samples with S5 representing pure sodalite octahydrate phase. The lack of analcime and NaP-1 phases in the XRD patterns implied the transformation of these unstable phases to a more stable phase of sodalite which is also well-known to be preferentially formed at high NaOH concentrations (Table 1) [24]. The obtained products showed high sodalite crystallinity. With increase in aging time to 2.5 h, not only the peaks associated to sodalite octahydrate were observed but also a new phase emerged which is marked with asterisk (Figure 5, S6). The newly appeared peaks can be well-identified as cancrinite. Due to the structural similarity between sodalite and

cancrinite, they can be synthesised under similar reaction conditions [25]. Also, the higher $\text{Na}_2\text{O}/\text{H}_2\text{O}$ molar ratio of the gel composition **b** (0.04) than gel composition **a** (0.02) favors the formation of cancrinite phase in the former mixture after enough aging time (Table 1) [26]. In addition, a slight decrease in peak intensity and a bit broadening can be seen in the XRD pattern (Figure 5, S6) suggesting the consumption of sodalite phase in favor of cancrinite and a change in size distribution of the crystals. These XRD results can clearly demonstrate that 1 h of stirring aging time is enough to obtain pure sodalite octahydrate phase and further aging time can lead to formation of disfavored new phase of cancrinite. Also, Debye-Scherrer formula was applied to calculate the particle size of this pure sodalite phase which resulted in ~ 30-40 nm (S5).

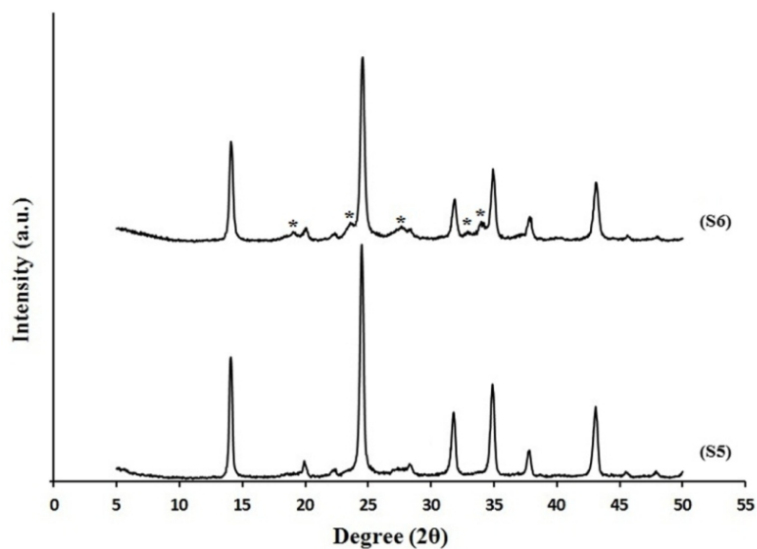


Fig.5. The XRD patterns of sodalite octahydrate samples of S5 and S6, prepared under 1 h and 2.5 h stirring aging from gel composition **b**, respectively. The cancrinite phase is denoted with asterisk.

The Fourier transform infrared (FT-IR) spectrum of pure nano-sodalite (S5) is shown in Fig. 6. The absorption band at $\sim 3500\text{ cm}^{-1}$ can be assigned to the stretching vibration of structural hydroxyl group (OH) of silicate lattice and the strongest vibration at $\sim 990\text{ cm}^{-1}$ is due to the asymmetric stretching mode of the tetrahedrally coordinated Si [14, 27]. The other 'fingerprint' absorptions were also observed at 524 and 465 cm^{-1} which correspond to the symmetric stretching mode of internal SiO_2 tetrahedra, and the structure-intensified T-O bending mode of tetrahedral TO_4 units (T= Al and Si), respectively. A diagnostic feature of the sodalite formation is the appearance of a new absorption peak at 434 cm^{-1} due to the formation of single four-membered ring (S4R) of sodalite unit [28].

The symmetric stretching vibrations (ν_s (T-O)) in the $670\text{-}730\text{ cm}^{-1}$ region are due to the symmetric stretch of T-O-T. Since these vibrations are sensitive to the mass of the anion and cation included in sodalite cage, the peak positions give an invaluable diagnostic for encapsulated molecules such as NaOH and H_2O [17, 29]. A sharp peak corresponding to the water deformation mode at $\sim 1650\text{ cm}^{-1}$ was appeared in the spectrum. Due to the strong hydrogen bonding, the central O...H stretching vibration is expected to be broader and shift to lower numbers. Therefore, the broad peak centered at absorption 1400 cm^{-1} can tentatively be assigned to this stretching vibration of O...H [17].

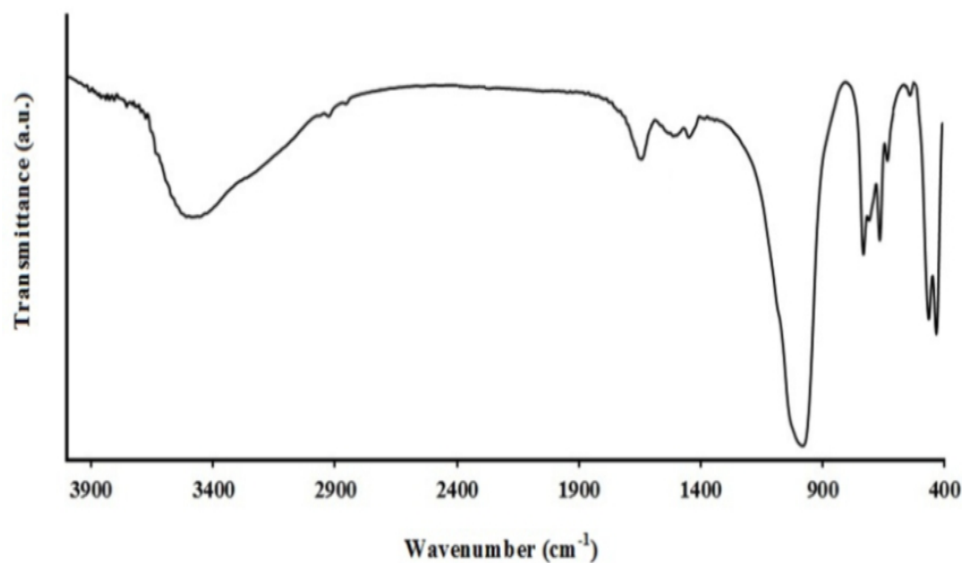


Fig.6. The FT-IR spectrum of sodalite octahydrate sample S5, prepared from gel composition **b** under 1 h of stirring aging.

Figure 7 illustrates the morphology and particle size of the samples S5 and S6. The FE-SEM image of S5 shows well-shaped spherical crystals of sodalite octahydrate with size distribution range of 50-80 nm which is in good agreement with Debye-Scherrer calculation.

The yield of the product based on SiO_2 was calculated to be about 15%. Also, the FE-SEM image of the mixed phases of sodalite and cancrinite shows nanosphere crystals in the range of 40-60 nm (Fig. 7, S6). The insets show the higher magnification images.

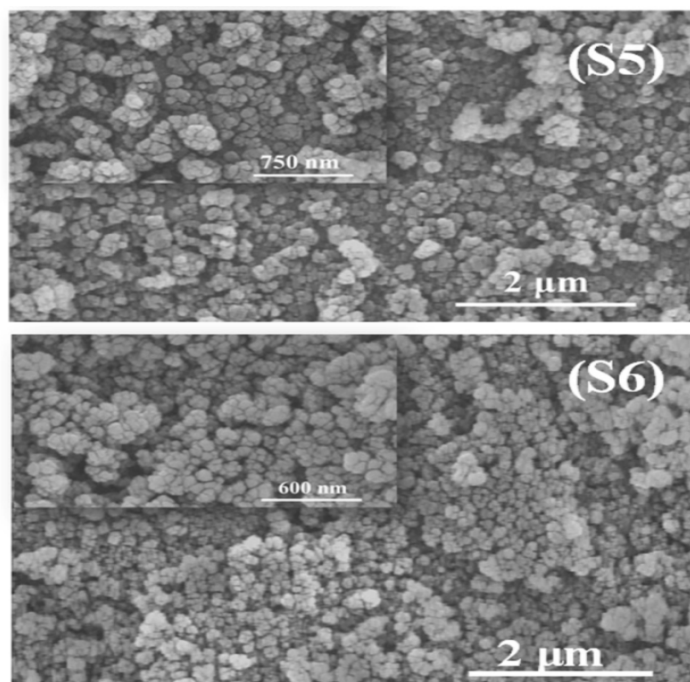


Fig.7. The FE-SEM images of samples S5 and S6, prepared from gel composition **b** under 1 h and 2.5 h of stirring aging, respectively.

The surface texture of the synthesised nanocrystalline sodalite (S5) was studied by argon adsorption-desorption isotherm. It should be noticed that the maximum window in the sodalite structure is 6R with a size of 0.28 nm. Therefore, N₂ adsorption-desorption isotherm is not useful to characterise the internal micropore [30] and only can roughly show the BET surface area coming from external surface of SOD particles [8]. Figure 8 shows the argon adsorption-desorption isotherm (a) and BJH method (b) analysis of sample S5. Figure 8a displays type II adsorption-desorption isotherm, being almost reversible. This type of isotherm

represents unrestricted monolayer-multilayer adsorption [31]. The results showed that the BET surface area (S_{BET}) of nanozeolite sodalite is 79.78 m² g⁻¹. The t-plot analysis showed that the obtained sample had very low micropore volume (< 0.002 cm³ g⁻¹) and external surface area very close to the S_{BET} value which indicated that the formation of microporous impurities in the sodalite sample was negligible. This type of isotherm represents unrestricted monolayer-multilayer adsorption [32-34]. Furthermore, the average pore diameter of 1.14 nm was obtained by BJH method (Figure 8b).

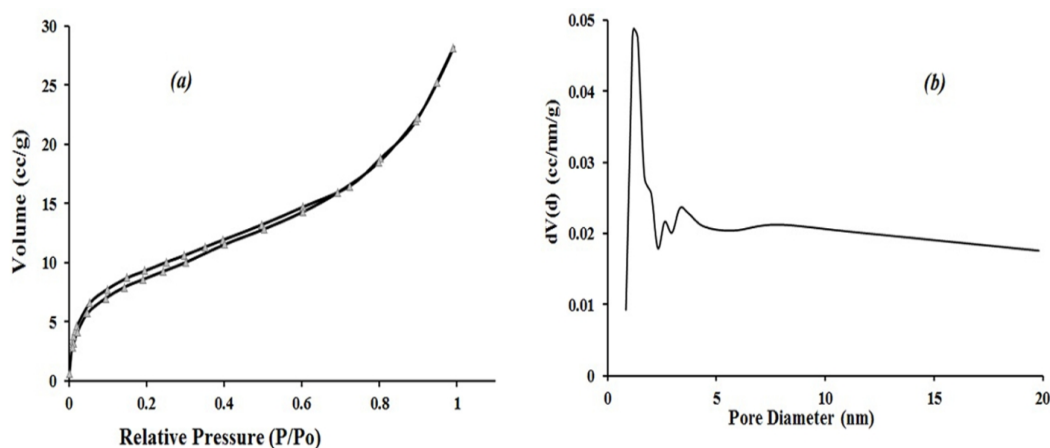


Fig.8. Argon adsorption-desorption isotherm (a) and BJH method diagram (b) of nanozeolite sodalite sample (S5)

4. CONCLUSION

In this work, a simple effective aging process was employed to control morphology and size distribution of sodalite by using two different initial gel compositions. The results indicated that stirring aging at room temperature prior to hydrothermal treatment can result in different morphologies in each gel mixture as well as reduction in particle size. With a Si/Al molar ratio of 5 and 20 min of aging time, microcrystals of sodalite with wool ball-like morphology was observed which had nano-threads (80-120 nm) and altered to cabbage-like microcrystals with 50-80 nm leaves by increasing in aging time to 72 h. On the other hand, sodalite nanocrystals of 50-80 nm were observed in high yield (~15%) with Si/Al molar ratio of 1.9 and 1 h aging time while prolonged aging time of 2.5 h led to formation of cancrinite as a new phase. The synthesized nanosodalite exhibited small particles which were evidenced by the broadening of XRD peaks, Debye-Scherrer calculation, FE-SEM

images and argon adsorption-desorption isotherm. Therefore, the stirring aging process is promising for simple synthesis of micro- and nano-crystalline sodalites.

Acknowledgements

The authors would like to thank Mrs. Mehrnoosh Sadeghi-Pari from Tehran University, Nano-electronic Laboratory for her infinite patience in FE-SEM measurements.

REFERENCES

- [1] K.L. Moran, W.T.A. Harrison, T.E. Gier, X. Bu, D. Herren, H. Eckert, G.D. Stucky, *Chem. Mater.* 8, 1930 (1996).
- [2] X.C. Xu, Y. Bao, C.S. Song, W.S. Yang, J. Liu, L.W. Lin, *Microporous Mesoporous Mater.* 75, 173 (2004).
- [3] A. Julbe, J. Motuzas, F. Cazevielle, G. Volle, C. Guizard, *Sep. Purif. Technol.* 32, 139 (2003).
- [4] J.C. Buhl, T.M. Gesing, C.H. Ruscher, *Microporous Mesoporous Mater.* 80, 57 (2005).

- [5] A. Stein, M. Meszaros, P.M. Macdonald, G.A. Ozin, G.D. Stucky, *Adv. Mater.* 3, 306 (1991).
- [6] A. Stein, G.A. Ozin, G.D. Stucky, *J. Am. Chem. Soc.* 112, 904 (1990)
- [7] D. Arieli, D.E.W. Vaughan, D. Goldfarb, *J. Am. Chem. Soc.* 126, 5776 (2004).
- [8] J.F. Yao, L.X. Zhang, H.T. Wang, *Mater. Lett.* 62, 4028 (2008)
- [9] S. Mintova, S.Y. Mo, T. Bein, *Chem. Mater.* 13, 901 (2001)
- [10] S. Mintova, N.H. Olson, T. Bein, *Angew. Chem., Int. Ed.* 38, 3201, (1999).
- [11] S. Mintova, N.H. Olson, V. Valtchev, T. Bein, *Science* 283, 958 (1999).
- [12] S. Mintova, V. Valtchev, *Stud. Surf. Sci. Catal.* 125, 141 (1999)
- [13] B.J. Schoeman, J. Sterte, J.E. Otterstedt, *Zeolites* 14, 208 (1994)
- [14] S.R. Lee, M. Park, Y.S. Han, J.H. Choy, *J. Phys. Chem. Solids* 65, 421 (2004).
- [15] S.R. Lee, M. Park, Y.S., Han, J.H. Choy, *Chem. Mater.* 15, 4840 (2003).
- [16] J.F. Yao, H.T. Wang, K.R. Ratinac, S.P. Ringer, *Chem. Mater.* 18, 1394 (2006).
- [17] W. Fan, K. Morozumi, R. Kimura, T. Yokoi, T. Okubo, *Langmuir* 24, 6952 (2008).
- [18] L. Tosheva, V.P. Valtchev, *Chem. Mater.* 17, 2494 (2005).
- [19] C.M. Zimmerman, A. Singh, W.J. Koros, *J. Membr. Sci.* 137, 145 (1997).
- [20] Z. Ghasemi, H. Younesi, H. Kazemian, *Can. J. Chem. Eng.* 89, 601 (2011).
- [21] A. Kuperman, S. Nadimi, S. Oliver, G.A. Ozin, J.M. Graces, M.M. Olken, *Nature* 365, 239 (1993).
- [22] S. Feng, T. Bein, *Science* 265, 1839 (1994).
- [23] F. Shi, X. Chen, L. Wang, J. Niu, J. Yu, Z. Wang, X. Zhang, *Chem. Mater.* 17, 6177 (2005).
- [24] J. Jiang, X.G.L. Feng, C. Duanmu, Y. Jin, T. Hu, J. Wu, *Powder Technol.* 217, 298 (2012).
- [25] M.T. Weller, *J. Chem. Soc. Dalton Trans.* 4227 (2000).
- [26] F. Ocanto, R. Álvarez, B. Moy, M. Brikgi, C. Urbina de Navarro, C.F. Linares, *J. Mater. Sci.* 43, 190 (2008).
- [27] B. Herreros, J. Klinowski, *J. Chem. Soc. Faraday* 91, 147 (1995)
- [28] D. Li, H.Y. Zhu, K.R. Ratinac, S.P. Ringer, H. Wang, *Microporous Mesoporous Mater.* 126, 14 (2009).
- [29] G. Engelhardt, J. Felsche, P. Sieger, *J. Am. Chem. Soc.* 114, 1173 (1992).
- [30] E.M. Flanigen, H. Khatami, H.A. Szymanski, *Am. Chem. Soc. Washington, DC*, (2009).
- [31] K.S.W. Sing, D.H. Everett, R.A.W. Haul, L. Moscow, R.A. Pierotti, J. Rouquérol, T. Siemieniewska, *Pure Appl. Chem.* 57, 603 (1985).
- [32] N. Hiyoshi, *Appl. Catal. A* 41, 164 (2012).
- [33] C. Grader, J.C. Buhl, *Microporous Mesoporous Mater.* 171, 110, (2013).
- [34] J.C. Buhl, K. Schuster, L. Robben, *Microporous Mesoporous Mater.* 142, 666 (2011).